Journal of Alloys and Compounds 525 (2012) 175–183

Contents lists available at SciVerse ScienceDirect

Journal of Alloys and Compounds

journal homepage: www.elsevier.com/locate/jallcom

Structural and magnetic transformations in $NdMn_2H_x$ hydrides

A. Budziak[a,*], P. Zachariasz[b], R. Pełka[a], H. Figiel[b], J. Żukrowski[b], M.W. Woch[b]

[a] The H. Niewodniczański Institute of Nuclear Physics PAN, ul. Radzikowskiego 152, 31-342 Kraków, Poland
[b] Faculty of Physics and Applied Computer Science, AGH, University of Science and Technology, al. Mickiewicza 30, 30-059 Kraków, Poland

ARTICLE INFO

Article history:
Received 10 November 2011
Received in revised form 31 January 2012
Accepted 1 February 2012
Available online xxx

Keywords:
Hydrogen in metals
Laves phase
Crystal structure
X-ray diffraction
Magnetic measurements

ABSTRACT

X-ray powder diffraction and bulk magnetization measurements were used to study structural and magnetic properties of hydrides $NdMn_2H_x$ ($2.0 \le x \le 4.0$). The X-ray investigations performed in the temperature range 70–385 K have revealed many structural transformations at low temperatures. In particular, a transformation from the hexagonal to the monoclinic phase and spinodal decompositions were observed. The magnetic behavior of the hydrides is correlated with the structural transitions. A tentative structural diagram is presented. The obtained results are compared with the properties of other cubic and hexagonal RMn_2H_x hydrides.

1. Introduction

The RMn_2 (R: rare earth and Yttrium) compounds crystallize mostly in two closely related structures of the Laves phase type: either in the cubic (*C15*) or in the hexagonal (*C14*) one. Both phases readily absorb hydrogen forming hydrides with hydrogen contents up to ~4.5 H/f.u., which induces strong modifications of their structural and magnetic properties. In recent years many different investigations of the RMn_2H_x (R: Y, Dy, Gd, Tb, Er, Sm and Ho) hydrides (both *C14* and *C15* type) have been carried out [1–8]. It is well established that hydrogen (deuterium) introduced into these compounds occupies tetrahedral A2B2 and AB3 sites [9–11]. The A2B2 sites are occupied by hydrogen atoms at low hydrogen concentrations (up to $x \sim 3.0$–3.5 H/f.u.), whereas for higher x the H atoms start to occupy the AB3 sites as well [12,13].

The research of the rare earth compounds with Mn shows an important role of the Mn–Mn nearest neighbor distance d which determines the magnetic interactions in the RMn_2H_x systems and leads to a variety of patterns of magnetic ordering. Above the critical value of $d_c \approx 2.7$ Å [14] a localized magnetic moment at the Mn sites is observed leading to a frustrated Mn sublattice [15]. The lattice parameters of the parent material $NdMn_2$ determined at room temperature are $a_{hex} \approx 5.567$ Å and $c_{hex} \approx 9.063$ Å implying that the Mn–Mn distance ($d_{Mn-Mn} \approx 2.74$ Å) is only slightly larger than the critical value d_c. Therefore, upon hydrogenation one should expect nontrivial magnetic structures in this system.

The present paper is a next step in a comprehensive work concerning the structural and magnetic properties of the RMn_2H_x hydrides. Its major aim is to report the structural and magnetic properties of $NdMn_2H_x$ and to compare them with those of other $RMn_2(H/D)_x$ [1–8,10,11]. The $NdMn_2$ compound, revealing at room temperature (RT) the hexagonal phase ($P6_3/mmc$), orders magnetically at ~104 K [16–18] and was found to absorb hydrogen very easily. Let us note that Nd here represents the lightest lanthanide reported so far in this context.

2. Experimental details

The host material $NdMn_2$ was prepared from high purity elements using the standard induction melting technique under argon atmosphere and annealing (1073 K, 5 days) to obtain a single-phase compound. The hydrogenation of the sample was carried out using the standard technology described in, e.g. [19]. Prior to hydrogenation the material was checked by X-ray diffraction (XRD) to determine the phase purity at RT. Like for other RMn_2H_x [1–8] the preparation of $NdMn_2H_x$ with hydrogen concentrations of 0.5–4.3 H/f.u. have been attempted at low hydrogen pressure (below ~2 bars). However, the samples with $x < 2.0$ H/f.u. consistently demonstrated the tendency to amorphization and multiphase behavior. For this reason only the results for the $NdMn_2H_x$ samples with concentrations $x = 2.0$, 2.5, 3.0, 3.5, and 4.0 H/f.u. are presented in this work.

The Siemens D5000 powder diffractometer with Cu Kα radiation ($\lambda = 1.54056$ Å) equipped with a continuous flow (LN_2) cryostat was used for the measurements of the lattice parameters in the temperature range 70–385 K. The data were collected on heating the samples. At each point the temperature was stabilized for ca. 40 min to reach the thermal equilibrium.

The FULLPROF program [20] based on the Rietveld method [21] was employed to analyze the X-ray diffraction patterns.

The DC susceptibility in the temperature range 77–300 K and for different applied fields (0.5 and 10 kOe) as well as the field dependence of the magnetization

* Corresponding author. Tel.: +48 12 662 8142; fax: +48 12 662 8458.
E-mail address: andrzej.budziak@ifj.edu.pl (A. Budziak).

0925-8388/$ – see front matter © 2012 Elsevier B.V. All rights reserved.
doi:10.1016/j.jallcom.2012.02.030

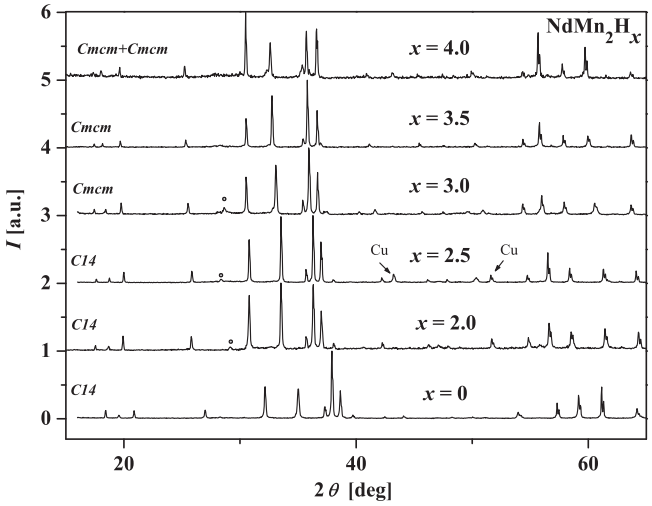

Fig. 1. XRD patterns as function of hydrogen concentration x for $NdMn_2H_x$ obtained at RT. Dots indicate the strongest lines of impurity phase NdO_2. Cu labels peaks corresponding to copper sample holder.

$M(H)$ in ±10 kOe field cycle at different temperatures were measured using the LakeShore VSM 7300 magnetometer.

In the paramagnetic state above the ordering temperature the measured susceptibilities of the $NdMn_2H_x$ hydrides were analyzed with the Curie–Weiss relation corrected for the diamagnetic contribution χ_{dia}: $\chi(T) = \chi_{dia} + C/(T - \Theta)$, where C is the Curie constant and Θ is the Weiss temperature.

3. Results

3.1. X-ray measurements

3.1.1. XRD patterns at 70 and 300 K

The XRD patterns obtained at RT, which served as a quality test for all the samples, are presented in Fig. 1. In the host material ($NdMn_2$) only trace amounts of impurities (NdO_2) were detected. Its lattice parameters obtained at 70 and 300 K (Table 1a and c) are in good agreement with the literature data [17,18]. Table 1a–c contains also the lattice parameters of all the analyzed $NdMn_2H_x$ hydrides obtained at 70, 265, and 300 K. All the hydrides contained small amount (below ~2% and 3%) of NdO_{2+x} and NdH_x impurities. According to the structure analysis only the samples with $x = 2.0$ and 2.5 H/f.u. reveal the *C14* single-phase of the host material at RT. The samples with $x = 3.0$ and 3.5 H/f.u. show a single orthorhombic phase, whereas the sample with $x = 4.0$ H/f.u. reveals the splitting into two orthorhombic phases with different hydrogen concentrations (Fig. 1 and Table 1a).

In contrast, at 70 K none of the hydrides sustains the *C14* phase of the host material. Almost all the samples show monoclinic phases, with the exception of the $NdMn_2H_{4.0}$ hydride where beside a monoclinic phase also an orthorhombic phase was revealed.

All the detected phases were described using three space groups: hexagonal ($P6_3/mmc$, no. 194), orthorhombic ($Cmcm$, no. 63), and monoclinic ($C2/m11$, no. 12). For the sake of comparison the lattice parameters of all the structures were converted to the pseudo-cubic system according to the relations: $a^*_{hex} = [(3)^{1/2}(a_{hex})^2 c_{hex}]^{1/3}$, $a^*_{orth} = [a_{orth}\, b_{orth}\, c_{orth}]^{1/3}$, $a^*_{mono} = [a_{mono}\, b_{mono}\, c_{mono}\, \sin(\alpha_{mono})]^{1/3}$ (Table 1a–c). As the same phase pattern was observed for $HoMn_2H_x$-*C14* [8], the same notation is preserved, i.e., β, γ, and ε for the *C14*, orthorhombic, and monoclinic phase, respectively.

As a result of hydrogen absorption a considerable expansion of the unit cell volume is observed. Table 1a shows the relative cell volume change $\Delta V/V_0$ for all the phases detected at 300 K. Its values

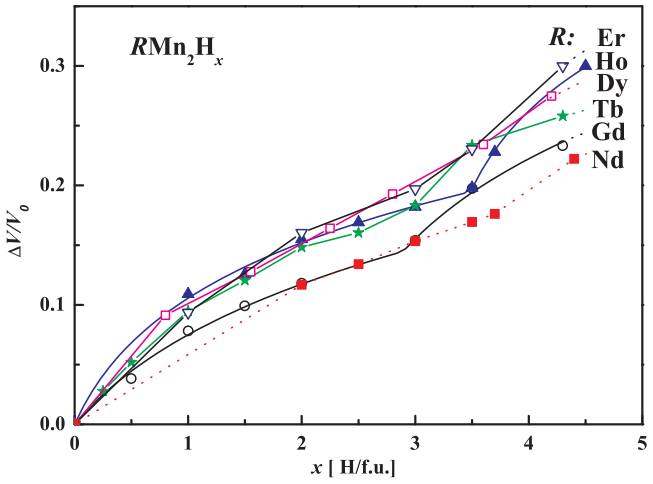

Fig. 2. Comparison of relative volume change of unit cell vs. x for various RMn_2H_x hydrides obtained at RT [8,13].

increase steadily with increasing hydrogen concentration attaining ~20% at $x = 4.0$ H/f.u. The lack of data points below $x < 2.0$ H/f.u., which is due to the instability and irreproducibility of the samples in this concentration region, precludes a reliable interpretation within the Hirata–Figiel model [13]. Nevertheless, it is instructive to compare the RT $\Delta V/V_0$ values obtained for $NdMn_2H_x$ to those reported for the other analyzed hydrides (Gd, Tb, Dy, Ho, Er)Mn_2H_x [8,13] (Fig. 2). For $x < 3.0$ H/f.u. there is an apparent gap between the data corresponding to $GdMn_2H_x$ and the remaining hydrides. It may be due to the difference in the electronic structure of the central Gd ion with the zero orbital angular momentum ground state and of the remaining rare earth ions with the vital orbital angular momentum contributions. Above $x \sim 3.5$ H/f.u. a dissimilar behavior is observed, especially at maximum hydrogen concentration (~4.5 H/f.u.) where the relative cell volume change $\Delta V/V_0$ increases monotonically with the atomic number of the rare earth element (Fig. 2). These findings clearly indicate that at elevated hydrogen concentrations for a heavier rare earth element in RMn_2H_x a slightly larger (by ~1%) unit cell expansion is to be expected. This hydrogen induced effect becomes at that high concentrations strong enough to mask the well known contraction of the ionic radii in the lanthanide series [22].

3.1.2. $NdMn_2$ and its hydrides with $2.0 \leq x \leq 4.0$

All the samples were measured in the temperature range 70–385 K assuming equal sampling intervals of 15 K. Fig. 3 shows a typical temperature evolution of the diffraction pattern detected for $HoMn_2H_{2.5}$ at low angles. The patterns were analyzed to yield the full set of the lattice parameters presented in Fig. 4 ($x = 2.0$ and 2.5 H/f.u.) and Fig. 5a–e ($x = 3.0$, 3.5 and 4.0 H/f.u.). Additionally, Fig. 5f combines the temperature evolutions of the pseudo-cubic lattice parameter a^* for all the samples.

For the samples with $x = 2.0$ and 2.5 H/f.u. similar structural transformations are observed. $NdMn_2H_{2.0}$ shows the *C14* phase (β) from the highest temperature down to ~270 K and then subsequently transforms to the orthorhombic one (γ) persisting down to ~235 K. At ~235 K a splitting occurs into two monoclinic phases ε_l and ε_h with low and high hydrogen content, respectively (Fig. 4b). This kind of splitting into two phases with different hydrogen contents is interpreted as a spinodal decomposition and was already reported for the other RMn_2H_x hydrides [1–8]. Using the relative abundances and the lattice parameters of the ε_l and ε_h phases the corresponding hydrogen concentrations are estimated as ~1.8 H/f.u. and ~2.8 H/f.u., respectively. The splitting

Table 1
Lattice parameters and refinement Rietveld factors obtained for $NdMn_2H_x$ at (a) 70 K, (b) 265 K, and (c) 295 K.

x [H/f.u.]			$x=0$	$x=2.0$		$x=2.5$		$x=3.0$	$x=3.5$	$x=4.0$		
				$x_l \approx 1.8$	$x_h \approx 2.8$	$x_l \approx 2.1$	$x_h \approx 2.8$			$x_l \approx 3.6$	$x_h \approx 4.6$	
Space group			$C2/m11$	$C2/m11$	$C2/m11$	$C2/m11$	$C2/m11$	$C2/m11$	$C2/m11$	$C2/m11$	$Cmcm$	
(a) 70 K												
Atom/site/coordinates	Nd1 $4i_1$	x	0	0	0	0	0	0	0	0	Nd $8f$	$x=0$
		y	0.661(2)	0.667(4)	0.670(3)	0.668(3)	0.637(2)	0.673(1)	0.664(2)	0.672(1)		$y=0.335(5)$
		z	0.939(1)	0.948(1)	0.953(2)	0.945(3)	0.932(1)	0.943(1)	0.936(1)	0.946(1)		$z=0.440(5)$
	Nd2 $4i_2$	x	0	0	0	0	0	0	0	0		
		y	0.329(2)	0.336(3)	0.333(3)	0.365(3)	0.338(1)	0.339(1)	0.331(2)	0.339(2)		
		z	0.435(2)	0.428(2)	0.431(3)	0.433(3)	0.433(1)	0.458(1)	0.430(2)	0.431(2)		
	Mn1 $2a$	x	0	0	0	0	0	0	0	0	Mn1 $4a$	$x=0$
		y	0	0	0	0	0	0	0	0		$y=0$
		z	0	0	0	0	0	0	0	0		$z=0$
	Mn2 $2c$	x	0	0	0	0	0	0	0	0	Mn2 $4c$	$x=0$
		y	0	0	0	0	0	0	0	0		$y=0.84(5)$
		z	½	½	½	½	½	½	½	½		$z=¼$
	Mn3 $8j$	x	0.751(1)	0.755(4)	0.754(4)	0.735(5)	0.762(4)	0.758(3)	0.765(3)	0.748(4)		
		y	0.078(1)	0.067(2)	0.067(4)	0.092(6)	0.086(2)	0.081(2)	0.080(2)	0.089(3)		
		z	0.237(2)	0.264(3)	0.264(4)	0.258(5)	0.259(2)	0.236(2)	0.239(4)	0.266(1)	Mn3 $8g$	$x=0.24(8)$
	Mn4 $4i$	x	0	0	0	0	0	0	0	0		$y=0.61(4)$
		y	0.165(2)	0.158(4)	0.156(6)	0.137(5)	0.159(4)	0.159(2)	0.161(2)	0.161(2)		$z=¼$
		z	0.746(2)	0.738(4)	0.738(6)	0.735(7)	0.751(4)	0.787(2)	0.757(4)	0.769(2)		
Abundance [%]			100	67(1)	33(1)	17(1)	83(1)	100	100	82(1)	18(2)	
Latt. par. a [Å]			5.5225(5)	5.727(2)	5.769(1)	5.780(2)	5.846(1)	5.883(1)	5.822(1)	5.815(1)	5.971(2)	
Latt. par. b [Å]			9.694(1)	10.031(2)	10.062(2)	10.045(2)	10.060(1)	10.061(1)	10.079(1)	10.081(1)	10.221(2)	
Latt. par. c [Å]			8.981(1)	9.388(1)	9.619(2)	9.386(1)	9.493(1)	9.483(1)	9.592(1)	9.726(1)	9.779(1)	
Angle α [°]			90.03(1)	90.25(4)	90.55(3)	90.56(3)	90.65(3)	90.10(2)	90.22(2)	90.21(2)	90.00	
V [Å^3]			480.7(1)	539.3(3)	558.3(3)	544.7(3)	558.2(3)	561.1(3)	562.9(3)	570.1(2)	596.8(4)	
a^* [Å]			7.835(5)	8.14(1)	8.23(1)	8.17(1)	8.23(1)	8.24(1)	8.26(1)	8.29(1)	8.42(1)	
a^*_w [Å]			7.834(5)	8.17(1)		8.22(1)		8.24(1)	8.26(1)		8.31(1)	
d_{Mn-Mn} [Å]			2.64(2)	2.71(6)	2.76(5)	2.72(5)	2.79(5)	2.77(3)	2.79(2)	2.77(3)	2.86(9)	
Bragg R-factor			11.6	15.3	12.1	13.1	10.6	11.1	11.3	12.7	14.3	
R_{wp}/R_{exp}			16.6/10.14	21.7/11.46		20.2/11.12		18.4/9.51	18.9/9.73		21.2/10.97	

x [H/f.u.]			$x=0$		$x=2.0$	$x=2.5$	$x=3.0$	$x=3.5$	$x=4.0$		
									$x_l \approx 3.65$		$x_h \approx 4.55$
Space group	$P6_3/mmc$				$Cmcm$	$Cmcm$	$Cmcm$	$Cmcm$	$Cmcm$		$Cmcm$
(b) 265 K											
Atom/site/coordinates	Nd $4f$	x	$x=1/3$	Nd $8f$	x 0	0	0	0	0		0
		y	$y=2/3$		y 0.326(2)	0.333(1)	0.338(2)	0.335(2)	0.336(3)		0.335(5)
		z	$z=0.067(1)$		z 0.435(2)	0.428(2)	0.429(3)	0.433(3)	0.438(1)		0.44(1)
	Mn1 $2a$	x	0	Mn1 $4a$	x 0	0	0	0	0		0
		y	0		y 0	0	0	0	0		0
		z	0		z 0	0	0	0	0		0
	Mn3 $6h$	x	0.831(1)	Mn2 $4c$	x 0	0	0	0	0		0
		y	$2x$		y 0.839(2)	0.839(1)	0.835(1)	0.842(5)	0.862(3)		0.840(5)
		z	¼		z ¼	¼	¼	¼	¼		¼
				Mn3 $8g$	x 0.257(2)	0.237(3)	0.236(4)	0.237(4)	0.239(4)		0.240(5)
					y 0.573(3)	0.557(2)	0.551(3)¼	0.568(3)	0.594(3)		0.58(1)
					z ¼	¼	¼	¼	¼		¼
Abundance [%]			100		100	100	100	100	76(1)		24(1)
Latt. par. a [Å]			5.5616(3)		5.767(1)	5.801(1)	5.819(1)	5.816(1)	5.818(1)		5.944(1)
Latt. par. b [Å]			5.5616(3)		9.989(1)	10.060(1)	10.078(1)	10.083(1)	10.081(1)		10.204(1)
Latt. par. c [Å]			9.0580(1)		9.392(1)	9.467(1)	9.560(1)	9.688(1)	9.734(1)		9.791(1)
V [Å^3]			242.6(1)		541.1(1)	552.5(1)	560.6(1)	568.1(1)	570.9(1)		593.5(1)
a^*; a^*_w [Å]			7.856(1)		8.148(1)	8.205(1)	8.245(1)	8.282(1)	8.296(1)	$8.32_w(2)$	8.40(1)
d_{Mn-Mn} [Å]			2.715(5)		2.73(5)	2.74(5)	2.75(4)	2.75(4)	2.78(5)		2.85(5)
Bragg R-factor			11.3		13.8	11.6	11.8	12.1	11.4		13.1
R_{wp}/R_{exp}			17.2/10.06		19.1/10.21	18.9/10.37	18.1/11.12	18.6/10.96	20.9/11.31		

into two phases characterized each by a relatively high hydrogen concentration were detected also for the other RMn_2H_x hydrides [3–6]. Let us note that the temperature dependence of the α_{mono} angles for ε_l and ε_h (Fig. 4c) reflect temperature dependent behavior of both phases leading to stable structural angles and relative concentrations when approaching 70 K.

A similar scenario of structural transformations, as for $x = 2.0$ H/f.u., was detected for the sample with $x = 2.5$ H/f.u. but the structural changes occur at slightly lower temperatures. The β phase exists from 385 K down to ~280 K whereupon it transforms to the γ phase. Below ~250 K the γ phase splits into two orthorhombic phases γ_l and γ_h with different hydrogen contents ~2.1 and 2.8 H/f.u., respectively (Fig. 4e). Below ~235 K both the orthorhombic phases transform to the monoclinic ones ε_l and ε_h, with $x_l \sim 1.9$ and $x_h \sim 2.9$ H/f.u., and persist down to the lowest temperatures. However, unlike for $x = 2.0$ H/f.u., no irregularities in the temperature behavior of the α_{mono} angle for ε_l or ε_h were observed, which supports the monoclinicity of both phases (Fig. 4f). The above

Table 1 (*Continued*)

x [H/f.u.]			$x=0$	$x=2.0$	$x=2.5$			$x=3.0$	$x=3.5$	$x=4.0$	
										$x_l \approx 3.7$	$x_h \approx 4.5$
Space group	$P6_3/mmc$			$P6_3/mmc$	$P6_3/mmc$			$Cmcm$	$Cmcm$	$Cmcm$	$Cmcm$
(c) 295 K											
Atom/site/ coordinates	Nd *4f*	x	1/3	1/3	1/3	Nd *8f*	x	0	0	0	0
		y	2/3	2/3	2/3		y	0.337(2)	0.338(2)	0.336(3)	0.335(5)
		z	0.065(1)	0.064(1)	0.064(1)		z	0.436(2)	0.435(1)	0.438(1)	0.44(1)
	Mn1 *2a*	x	0	0	0	Mn1 *4a*	x	0	0	0	0
		y	0	0	0		y	0	0	0	0
		z	0	0	0		z	0	0	0	0
							x	0	0	0	0
						Mn2	y	0.839(1)	0.840(3)	0.835(3)	0.835(5)
	Mn3 *6h*	x	0.832(1)	0.837(1)	0.835(1)	*4c*	z	¼	¼	¼	¼
		y	$2x$	$2x$	$2x$						
		z	¼	¼	¼	Mn3	x	0.259(2)	0.256(3)	0.256(4)	0.248(6)
						8g	y	0.579(3)	0.578(1)	0.577(3)	0.575(7)
							z	¼	¼	¼	¼
Abundance [%]			100	100	100			100	100	74(1)	26(1)
Latt. par. a [Å]			5.5672(3)	5.774(1)	5.802			5.822	5.820	5.823	5.944(2)
Latt. par. b [Å]			5.5672(3)	5.774(1)	5.802			10.076	10.085	10.082	10.209(1)
Latt. par. c [Å]			9.0633(2)	9.409(1)	9.462			9.563	9.691	9.737	9.798(1)
V [Å^3]			243.3(1)	271.7 (1)	275.8(1)			561.0(2)	568.8(2)	572.2(2)	594.6(3)
a^* [Å]			7.864(1)	8.159(2)	8.201(2)			8.247(2)	8.285(2)	8.301(2)	8.408(3)
$\Delta V/V_0$ [%]			–	0.116(1)	0.134(1)			0.153(1)	0.169(1)	0.176(1)	0.222(1)
d_{Mn-Mn} [Å]			2.74(2)	2.82(3)	2.86(3)			2.80(5)	2.80(5)	2.83(3)	2.87(5)
Bragg R-factor			10.9	10.8	9.8			10.6	10.1	10.6	12.1
R_{wp}/R_{exp}			17.8/10.43	19.7/10.6	18.9/11.1			18.0/10.79	18.1/11.01	19.9/11.86	

a^* and a^*_w – non and weighted pseudo-cubic lattice parameters, respectively.

transformations are illustrated in Fig. 6 in terms of the evolution of the hexagonal line (2 0 5).

For the samples with $x=3.0$ and 3.5 H/f.u. no spinodal decompositions were observed. Only the structural transformations of the $\beta \rightarrow \gamma \rightarrow \varepsilon$ type were detected at ~310 and ~250 K and ~325 and ~205 K for $x=3.0$ and 3.5 H/f.u., respectively (Fig. 5). Fig. 7 presents the diffraction lines of the $NdMn_2H_{3.0}$ sample at three temperatures: 340 K, 265 K, and 70 K which correspond to the hexagonal, orthorhombic, and monoclinic phases, respectively. The most intense lines are indexed. The lattice parameters of the hexagonal phase at 340 K are: $a_h = 5.8333(2)$ Å, $c_h = 9.5884(3)$ Å, and for the other phases are collected in Table 1a and b. Relatively high R-factors are typical for the patterns of the RMn_2H_x hydrides when obtained with the XRD diffractometer equipped with Cu-anode lamp.

Diffraction lines of the orthorhombic phase (Fig. 7b) are slightly broadened and show lower intensities in comparison to the hexagonal phase lines (Fig. 7a). In turn, Fig 7c presents already clearly visible splits of reflections of the monoclinic phase. The refinement of the XRD patterns of the hydrides with $x=3.0$ and 3.5 H/f.u. were the basis for the refinements of the other two-phase hydrides, especially these with $x=2.0$ and 2.5 H/f.u. where overlapped lines can mask the individual behavior of the phases.

For the $NdMn_2H_{4.0}$ sample a coexistence of two phases in the whole temperature range 70–385 K was found. Both phases undergo independent structural transformations on lowering temperature. The phase with subscript '*l*' corresponds to a lower hydrogen concentration (~3.6 to 3.7 H/f.u.), whereas the other one with subscript '*h*' corresponds to a higher hydrogen content (~4.4 to 4.6 H/f.u.). A spinodal decomposition above the highest temperature accessible experimentally may be anticipated.

In general, the temperature dependences of the lattice parameters for all the hydrides discussed here are rather irregular and non-monotonic, except for the temperature ranges where the hexagonal phases are detected. Apparently, in Fig. 5f showing the temperature dependence of the pseudo-cubic lattice parameter a straight line separating the γ and β phases can be drawn (the dotted line). A similar observation was made for $HoMn_2H_x$ *C15* and *C14* with $x \geq 2.0$ H/f.u. [7,8].

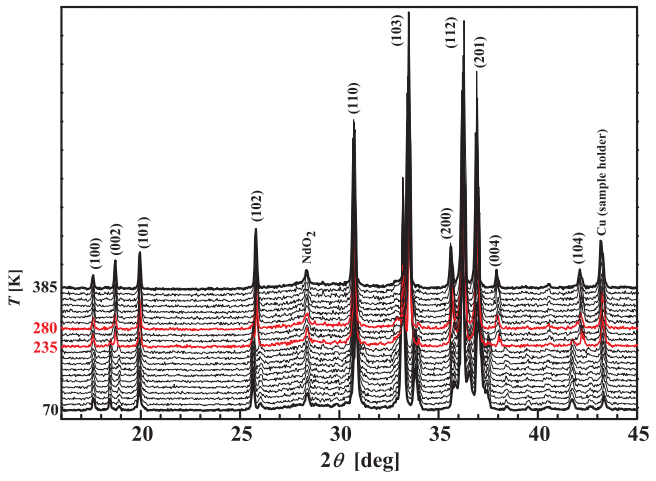

Fig. 3. Temperature evolution of diffraction lines for $NdMn_2H_{2.5}$. Additional lines come from NdO_2 oxide and form copper sample holder.

3.2. Magnetic properties

3.2.1. M(T) measurements

The thermal dependence of the magnetization $M(T)$ in the external field of 0.5 and 10 kOe is presented in Fig. 8 for all the hydrides. Both the low-field and the high-field data show a variable behavior reflecting the structural changes of the samples with temperature. The measurements enable to estimate the temperatures of magnetic transitions $T_{N,C}$. Moreover, for $x=2.5$ and 3.0 H/f.u. the effective moments per formula unit $\mu_{eff} = (3k_B C_{mol}/N(\mu_B)^2)^{1/2}$ as well as the Weiss temperature Θ were determined using the Curie–Weiss law in the high-temperature paramagnetic regime for the 10 kOe field data. The results are compared with those for the host material $NdMn_2$ [16] and listed in Table 2. The individual

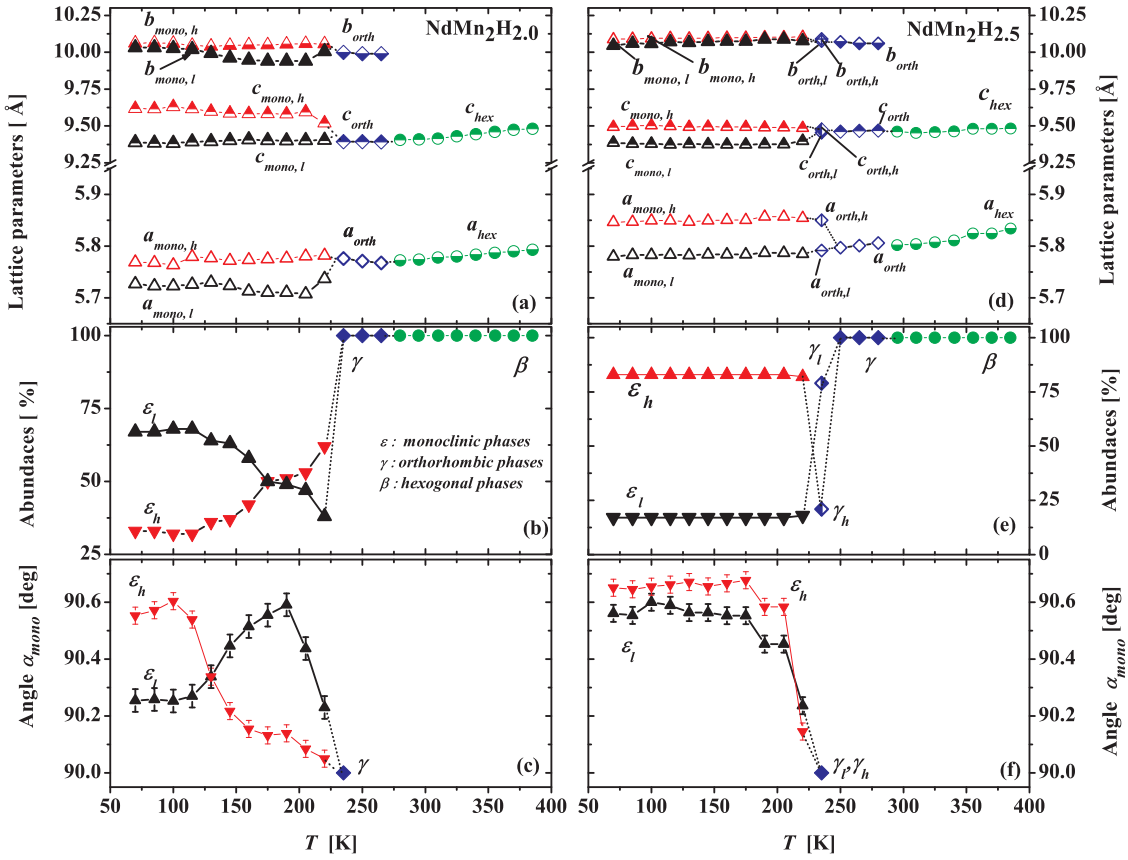

Fig. 4. Full set of unit cell parameters and relative phase abundances for $NdMn_2H_{2.0}$ (a–c) and $NdMn_2H_{2.5}$ (d–f) as function of temperature. If it is not marked in the other way, the error bars are not bigger than the font size.

effective moment of the Nd^{3+} free ion is 3.62 μ_B [16]. It is substantially smaller than the values found for the hydrides with $x = 2.5$ and 3.0 H/f.u (~5.0 μ_B and ~4.5 μ_B, respectively) and it exceeds the value of ~2.0 μ_B reported for Nd atom in $NdMn_2$ [17]. The latter fact is understandable as the crystal field effects at the Nd ion are expected to suppress the value of its magnetic moment. The large discrepancies between the detected values of μ_{eff} and the expected value for Nd^{3+} confirm the presence of finite magnetic moments at the Mn sites. Assuming the value of $\mu_{Nd} = 2.0\ \mu_B$ and using the relation $\mu_{eff} = [2(\mu_{Mn})^2 + (\mu_{Nd})^2]^{1/2}$ one can estimate the magnetic moment of the Mn site μ_{Mn} as equal to ~3.2 μ_B and ~2.8 μ_B, respectively. These values are higher than the value of 2.4 μ_B found from the neutron diffraction experiment for $NdMn_2$ [17]. This can be attributed to the fact that in the hydrogenated samples the Mn–Mn distance is larger than in the host material giving rise to a better stabilization of the Mn moments and an ensuing increase in their magnitudes.

It can be seen that on lowering temperature the magnetic transitions usually follow the structural transformations detected in the samples, reflecting the presence of the correlation between the structural changes and the magnetic interactions in the compounds under study. One can presume that this rather complex magnetic behavior of the hydrides is a result of the peculiar property of the host $NdMn_2$ material showing the spin reorientation at 50 K [17]. At the same time, a substantial increase of the magnetic ordering temperatures with increasing hydrogen content should be attributed to the primary role played by the manganese sublattice in the determination of the $NdMn_2H_x$ magnetism. This is due to the relatively more accessible and unshielded character of the 3d electrons as compared to those residing in the 4f rare earth shell. The gradual extension of Mn–Mn distances, taking place in the process of increasing hydrogen content, is expected to enhance considerably the magnitude of exchange interactions within this sublattice. Magnetic moments on the Mn sites become more and more localized and thus boost the stabilization of the magnetically ordered phase. In the following subsections it will be discussed in detail.

Table 2
Magnetic parameters in the paramagnetic state at $H = 10$ kOe and temperatures of structural transformations of $NdMn_2H_x$ hydrides.

x [H/f.u.]	μ_{eff} [μ_B/f.u.]	θ [K]	$T_{N,C}$ [K]	$T_S \pm 10$ [K]
0.0	4.1[a]	37[a]	104[a]	107
2.0	–	–	245 ± 3	235, 265
2.5	5.0 ± 1.0	210 ± 40	250 ± 5	235, 250, 280
3.0	4.0 ± 1.0	200 ± 50	265 ± 5	250, 300
3.5	–	–	275 ± 15	205, 315
4.0	–	–	>300[b]	130[c], 330[c], 360[d]

T_S – temperature of structural transformation (underbars mark transformation $\gamma \rightarrow \beta$).
[a] Ref. [16].
[b] Expected temperature range.
[c] Phase with low hydrogen content.
[d] Phase with high hydrogen content.

3.2.1.1. Hydrides with $2.0 \leq x \leq 3.0$. The shapes of the $M(T)$ curves for the samples with $x = 2.0$, 2.5 and 3.0 H/f.u. are roughly similar (Fig. 8). The main difference lies in the magnitude of the magnetization of $NdMn_2H_{3.0}$ revealing definitely the strongest signal. This is consistent with the gradual expansion of the lattice due to hydrogenation and the anticipated stabilization of the magnetic moments on the Mn sites. Both in low and high magnetic field characteristic jumps/inflections in the $M(T)$ curves appear between 120 and 140 K followed by broad plateaus and relatively sharp magnetization

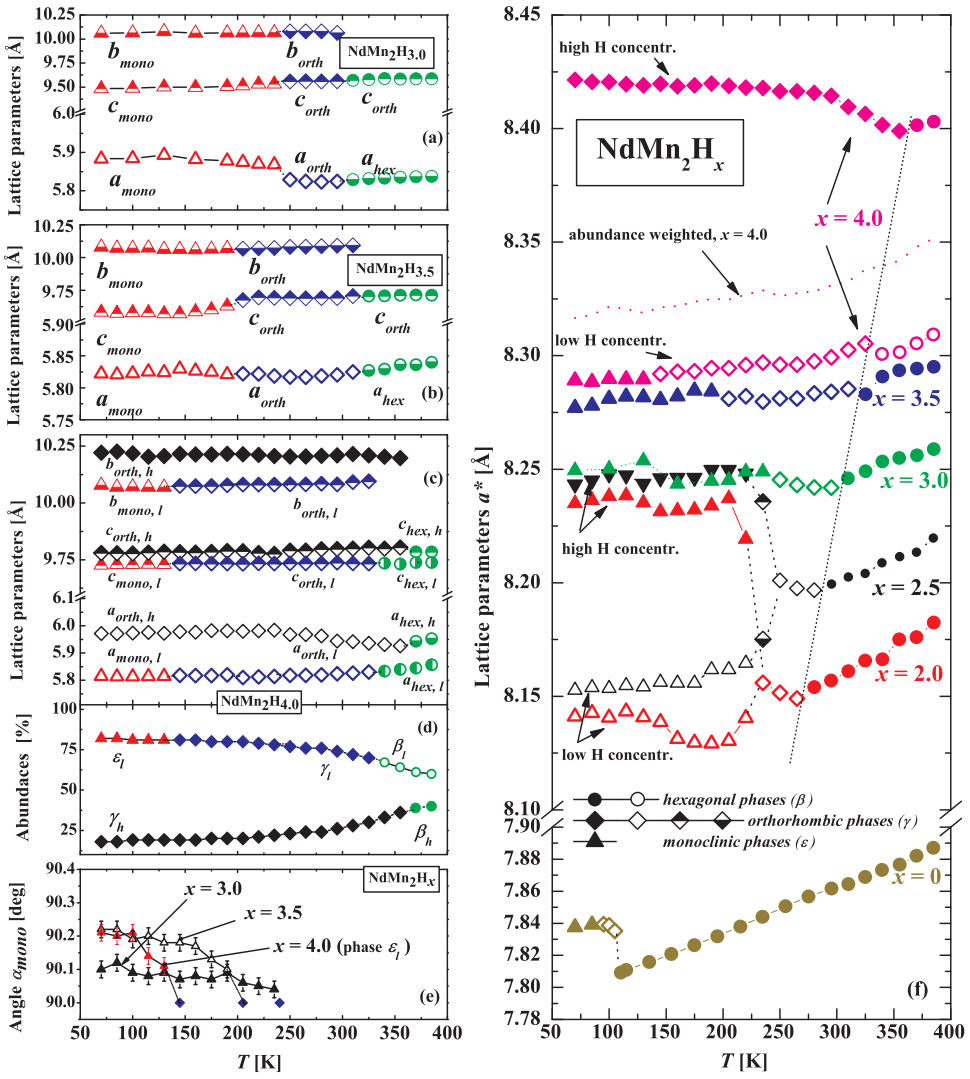

Fig. 5. (a–e) Unit cell parameters and relative phase abundances for $NdMn_2H_x$ (x = 3.0, 3.5, 4.0 H/f.u.) as function of temperature; (f) Pseudo-cubic lattice parameters of all analyzed $NdMn_2H_x$ samples (see Section 3.1 for details). If it is not marked in the other way, the error bars are not bigger than the font size.

drops at the magnetic ordering temperatures. The magnetic ordering temperature ($T_{N,C}$) rises with increasing x and amounts to ~245, ~250 K, and as much as ~265 K for x = 2.0, 2.5 and 3.0 H/f.u., respectively.

In order to rationalize the observed thermal evolution of the net magnetic moment of the samples one has to keep in mind the findings of the structural analysis. For x = 2.5 H/f.u. at ~235 K the splitting into two phases (ε_l and ε_h) with different hydrogen contents of ~1.9 and ~2.9 H/f.u. was clearly observed. Let us assume that the phase with lower x (ε_l) is a collinear antiferromagnet like it was the case for the (Gd,Tb)Mn_2H_x hydrides with x = 2.0 H/f.u. [3,4] which was confirmed by neutron diffraction [10]. The ε_h phase seems then to be of the ferrimagnetic type. Consequently, the x = 3.0 H/f.u. sample should be considered as a ferrimagnet like the hydrogen rich ε_h phase, which is corroborated by the obtained results. However, the mass magnetization of the hydrogen rich phase ε_h calculated on the basis of the abundances of ε_l and ε_h in the x = 2.5 H/f.u. sample (Fig. 4e) amounts to ~1.3 G cm^3/g. It is one order of magnitude lower than the value of ~13.0 G cm^3/g (Fig. 8b) detected in the x = 3.0 H/f.u. sample in this temperature range. This indicates that both phases are not magnetically equivalent and/or the compounds show a high sensitivity to hydrogen concentration. The latter fact seems to be further confirmed by the case of the x = 2.0 H/f.u. sample, where despite the same crystal symmetries of the ε_l and ε_h phases and an essentially different thermal evolution of their abundances (Fig. 4b), roughly the same value of the magnetization at 150 K ≤ T ≤ 230 K (~1.0 G cm^3/g) is observed. The different $M(T)$ evolution for both x for T < 150 K reflects probably the complexity of the abundance behavior. The fact that the low temperature magnetization for x = 2.0 H/f.u. exceeds that of x = 2.5 suggests that even the ε_l phase acquires a comparable nonzero net magnetization, which is in line with our earlier presumption of a higher structural symmetry of the ε_l phase. The characteristic $M(T)$ increase detected for both hydrides at ~120 to 130 K implies some reorganization of the magnetic order involving a possible spin reorientation process of the Nd and Mn sublattices. A similar behavior was observed for the cubic hydrides/deutrides [23].

3.2.1.2. Hydrides with x = 3.5 and x = 4.0.. The magnetization curve for x = 3.5 H/f.u. is strongly correlated with the structural transformations of that hydride discussed in Section 3.1. The low-field magnetic anomaly with the maximum at 180 K follows closely the lowering of symmetry of the unit cell at ~190 K ($\beta \rightarrow \gamma$). At ~150 K slight irregularities of the lattice parameters (a_{mono} and c_{mono}) are observed (Fig. 5b) signaling a possible reorganization of the magnetic order. The magnitude of the magnetization for the x = 3.5 H/f.u.

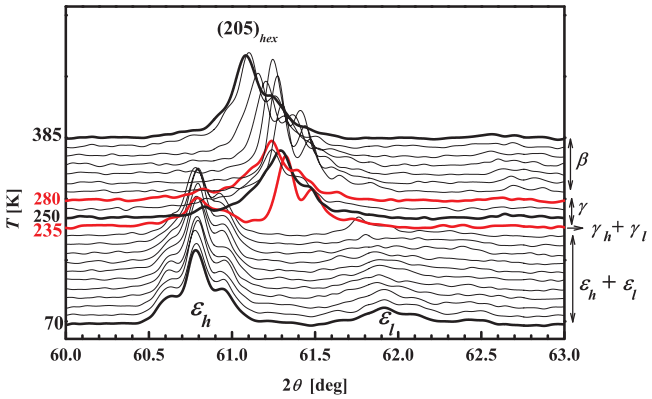

Fig. 6. Temperature evolution of diffraction line $(2\,0\,5)_{hex}$ for $NdMn_2H_{2.5}$ with marked intervals of structurally different phases.

and $x = 3.0$ H/f.u. samples are substantially different implying a different type of magnetic ordering linked with a possible change of the magnitudes of the local moments on the Mn and Nd sites. The latter feature may be attributed to the fact that at this high hydrogen concentration the AB3 interstitial sites start to be filled. A similar behavior was reported for the other RMn_2H_x hydrides [13]. The experimental temperature limit precludes the determination of magnetic ordering temperature $T_{N,C}$. In the next paragraph dealing with hysteresis loops it will be argued that the sample with $x = 3.5$ H/f.u. at $T = 290$ K is already in the paramagnetic state.

The two-phase hydride $NdMn_2H_{4.0}$ shows two magnetic anomalies in the low-field measurement at ~95 K and ~110 K (Fig. 8c). Both peaks are rather weekly related to the

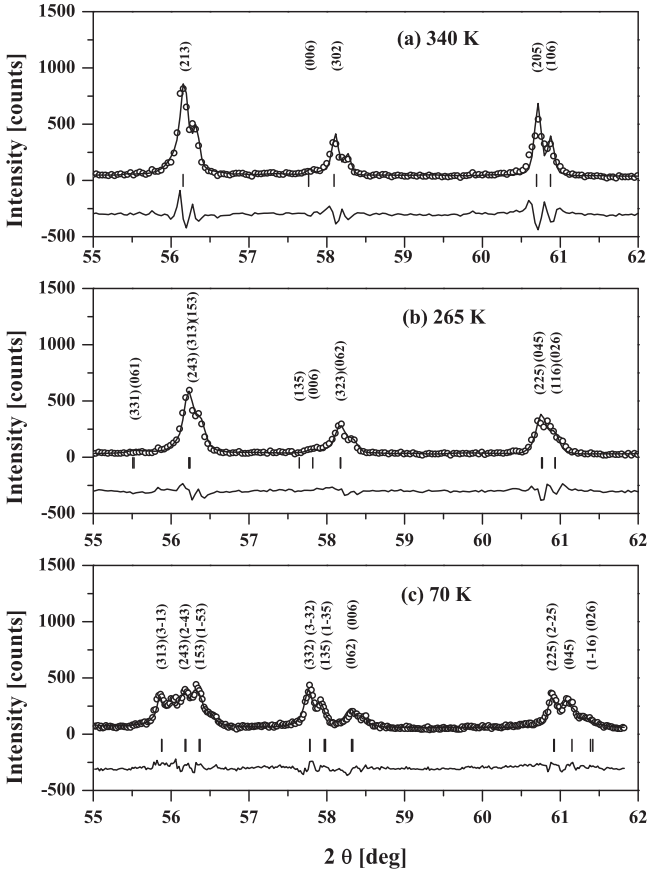

Fig. 7. Parts of the XRD patterns for $NdMn_2H_{3.0}$ taken at (a) 340 K, (b) 265 K, and (c) 70 K correspond to hexagonal, orthorhombic, and monoclinic structures.

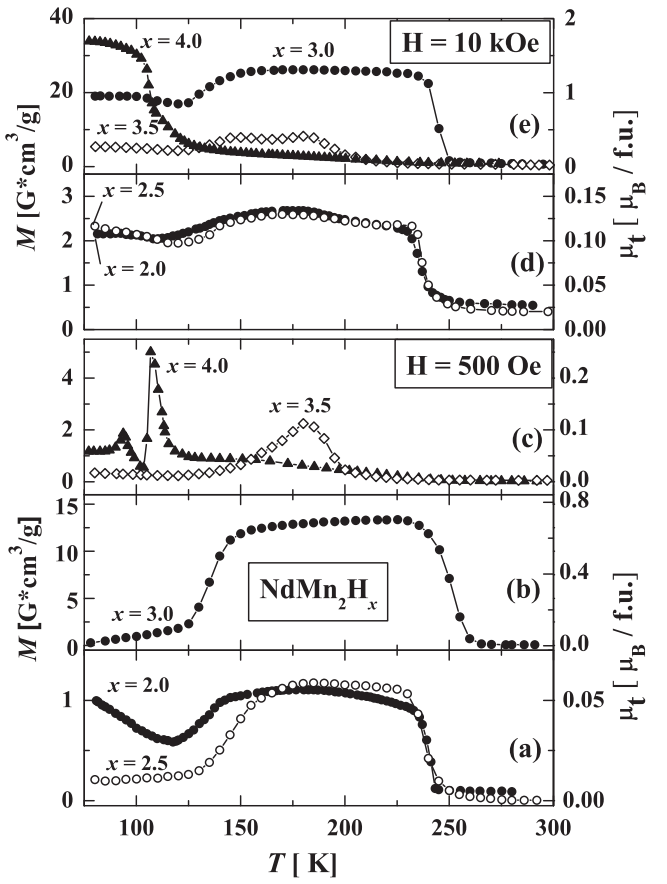

Fig. 8. Magnetization of $NdMn_2H_x$ hydrides vs. T in external field of 0.5 and 10 kOe.

structural transformations. Only small irregularities in the temperature dependence of the abundance weighted pseudo-cubic lattice parameter a^* can be noticed (Fig. 5f, the dotted line) which mainly come from the wave-like feature in the lattice parameter b_{mono} vs. T detected in this temperature region (Fig. 5c). The low temperature peak disappears in the external field of 10 kOe and is replaced by a regular elevated signal falling abruptly at the temperature corresponding to the high temperature peak. The magnetization signal above ~120 K (in both 0.5 and 10 kOe) decreases smoothly up to the temperature limit of the measurement (Fig. 8e). It suggests, like for the other $RMn_2(H/D)_{4.0–4.5}$ hydrides/deuterides [3–5,24], that the magnetic ordering temperatures of both phases should be observed above 300 K. The $NdMn_2H_{4.0}$ hydride shows the largest value of magnetization below 100 K of all the hydrides, which can be attributed to a presumable spin reorientation process in the ε_h phase. Owing to the fact that the system is two phased and due to the lack of magnetic measurements for hydrides with the nominal hydrogen concentration above $x = 4.4$ H/f.u. it is very difficult to unravel the magnetic behavior of both constituent phases (ε_l and ε_h).

3.2.2. *M(H) measurements*

Fig. 9 shows the magnetization curves $M(H)$ and/or hysteresis loops for the single-phase samples with $x = 3.0$ and 3.5 H/f.u. at various temperatures. It is apparent that the applied field of 10 kOe is still insufficient to orient the Nd and Mn magnetic moments parallel to the field direction in both hydrides. The high temperature data (290 K) confirm that the sample is in a paramagnetic state ($x = 3.0$ H/f.u.) or close to it ($x = 3.5$ H/f.u.).

The hysteresis loops obtained at 77 K are rather wide, the coercive fields are 2.6 kOe and 2.0 kOe for $x = 3.0$ and 3.5 H/f.u.,

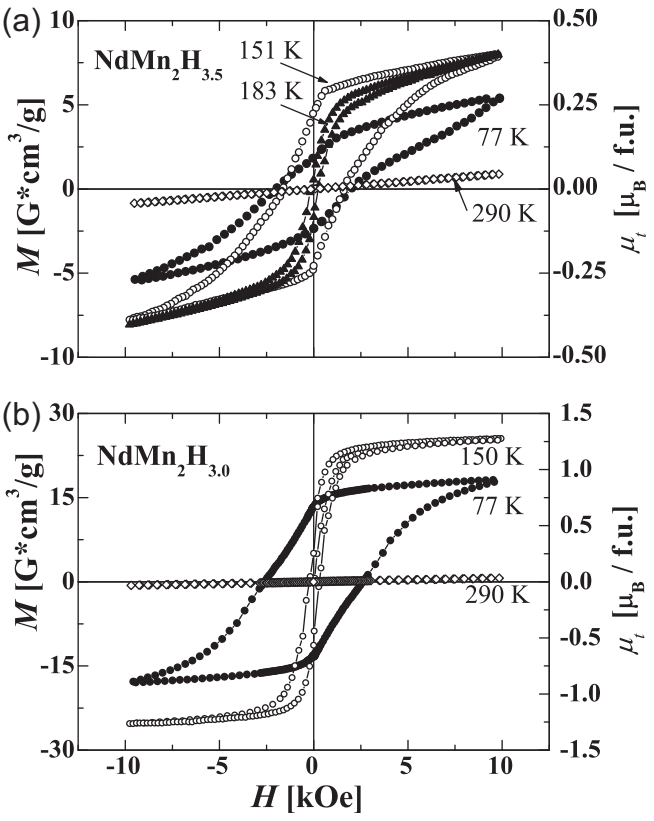

Fig. 9. Magnetization curves vs. external field for single-phase $NdMn_2H_{3.0}$ (a) and $NdMn_2H_{3.5}$ (b) hydrides at different temperatures.

respectively. Such shapes of the hysteresis loops indicate a ferro- or ferrimagnetic ordering in the low temperature phases of the samples and the presence of the considerable magneto-crystalline anisotropy.

At 150 K for $x = 3.0$ H/f.u. and at 183 K for $x = 3.5$ H/f.u. the $M(H)$ curves behave in a different way. They are relatively narrow, which may point to a rearrangement of the magnetic moments in the samples. Such a behavior confirms the previous suggestions of complicated magnetic structures in both the hydrides. Interestingly, there is a threefold change of the magnetization magnitude of both

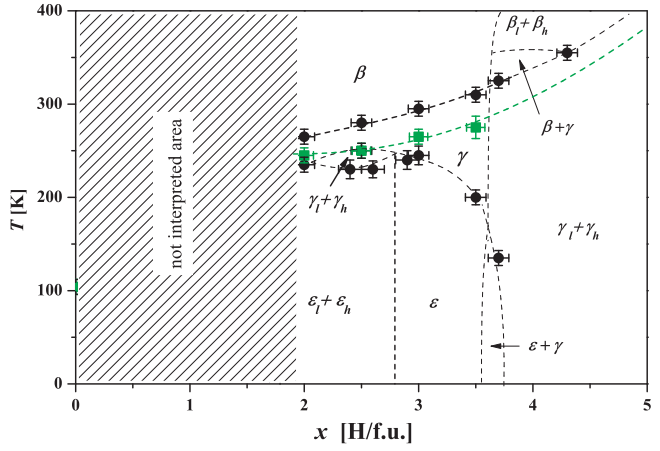

Fig. 10. Tentative structural phase diagram for $NdMn_2H_x$ hydrides. Squares correspond to magnetic ordering temperatures. Green dashed line separates paramagnetic and magnetically ordered states. Symbols β, γ, and ε denote hexagonal, orthorhombic and monoclinic phase, respectively. (For interpretation of the references to color in this figure legend, the reader is referred to the web version of this article.)

hydrides at the corresponding temperatures (Fig. 9). This may be rationalized if one assumes that in the phases of the $x = 3.5$ H/f.u. hydride the magnetic moments at the two Mn sites are approximately parallel and that at the Nd site is antiparallel (↑↓↑), whereas in those of the $x = 3.0$ H/f.u. hydride the magnetic moments at all the sites are roughly parallel (↑↑↑). It is clear that these arrangements would account for the threefold difference in the magnitude of the magnetization, if only the magnetic moments at all the sites are comparable. This condition may well be fulfilled because the plausible values of the Mn magnetic moment in this class of compounds fall in the range of 2.5–3.5 μ_B, whereas the upper limit for the Nd magnetic moment is ~3.7 μ_B.

4. Conclusions

Taking into account the XRD results it was possible to draft a structural phase diagram for the $NdMn_2H_x$ hydrides (Fig. 10). In comparison to the other (Gd,Tb,Er,Ho)Mn_2H_x [3–5,7,8] compounds the area for $x < 2.0$ H/f.u. is missing, which is due to the difficulties in obtaining stable and reproducible hydrides in this concentration range. The analysis of the XRD patterns for the hydrides with such a low hydrogen content indicated also a high level of amorphization of the samples. A similar behavior was observed for the $SmMn_2H_x$ hydrides with $x < 2.0$ H/f.u. [25], which can suggest that the RMn_2H_x hydrides with light lanthanides do not create stable compounds with low-hydrogen concentrations.

For all the examined hydrides the structural transformations share the same phase sequence from the high-temperature hexagonal phase via the orthorhombic one and finally to the monoclinic one ($\beta \rightarrow \gamma \rightarrow \varepsilon$). The $NdMn_2H_x$ samples with $x = 2.0$ and 2.5 H/f.u. split into two phases with different hydrogen contents. It is worth noting that the (Gd,Tb,Er,Ho)$Mn_2H_{2.0}$ hydrides reveal a single-phase in the whole temperature range [3–5,7,8], whereas a spinodal decomposition into two phases (with $x_l \sim 1.9$ and $x_h \sim 2.1$ H/f.u.) was observed for $SmMn_2H_{2.0}$ only [6]. This observation makes a clear distinction between RMn_2H_x hydrides with light and heavy lanthanides. It is also surprising that the ε_h or particularly ε_l phases in $NdMn_2H_{2.0}$ and $NdMn_2H_{2.5}$ should not be equivalent (Fig. 5f). One could expect that the corresponding phases would have the same hydrogen concentrations similarly to what was observed for (Gd,Tb,Er,Ho)Mn_2H_x with $x < 2.0$ H/f.u. [3–5,7,8].

Only the samples with $x = 3.0$ and 3.5 H/f.u. reveal a single-phase in the whole temperature range keeping, however, the same structural transformation sequence $\beta \rightarrow \gamma \rightarrow \varepsilon$.

In turn, for the sample with the highest nominal hydrogen concentration $x = 4.0$ H/f.u. two phases with different hydrogen contents are observed in the whole temperature range following probably a spinodal decomposition located somewhere above 385 K. Such a behavior was also reported for $ErMn_2H_{4.3}$ [5].

Unusually complicated structural transitions of the $NdMn_2H_x$ hydrides are reflected in the magnetic results. Since most of the samples are two-phased, the construction of even a tentative magnetic phase diagram is no mean feat. The only thing one can be reasonably sure of is the location of the transitions from the paramagnetic to the ordered state. Hence, for the sake of comparison, the estimated values of $T_{N,C}$ (see Table 2) are plotted as green squares in the structural phase diagram (Fig. 10). A green dotted line was drawn to separate the paramagnetic from the magnetically ordered states. One can see that the temperatures of the structural transformations of the $\beta \rightarrow \gamma$ type and those of the magnetic ordering transitions do not coincide with the latter being slightly lower than the former.

Such high $T_{N,C}$ were also observed and reported for the other RMn_2H_x hydrides [3–8] and can be likewise explained as due to the hydrogen induced shift of the Mn–Mn distances above the critical

distance for the stabilization of the magnetic moment at the Mn sites. It leads to a better localization of the Mn magnetic moments and in consequence to a strong increase of the magnetic ordering temperature. The magnetic properties of the $NdMn_2H_x$ hydrides are generally governed by a relative importance of the Mn–Mn, Mn–Nd and Nd–Nd exchange interactions. The improving stability of the Mn moments along with the increasing strength of the Mn–Mn coupling cause an increase of $T_{N,C}$ with x.

Table 1a–c shows that the distance $d_{Mn-Mn} < 2.7$ Å is observed only for the host material $NdMn_2$ at 70 K. For all its hydrides the distance is higher than 2.7 Å and shows tendency to increase with growing hydrogen content and temperature what well correlates with increasing magnetic ordering temperature related to localization of Mn moments and their exchange interaction.

The results reported in the present paper form the solid basis for further more elaborate studies of this striking class of compounds. Providing a crucial insight into the phase behavior they are still far from sufficient to unravel the detailed magnetic structure. To gain a definite knowledge of the patterns of magnetic ordering and the magnitudes of the constituent magnetic moments one should refer to the technique of neutron diffraction. Such experiments are currently in progress and will be reported elsewhere.

References

[1] H. Figiel, J. Przewoźnik, V. Paul-Boncour, A. Lindbaum, E. Gratz, M. Latroche, J. Alloys Compd. 274 (1998) 29.
[2] J. Przewoźnik, J. Żukrowski, K. Freindl, E. Japa, K. Krop, J. Alloys Compd. 284 (1999) 31.
[3] J. Żukrowski, H. Figiel, A. Budziak, P. Zachariasz, G. Fisher, E. Dormann, J. Magn. Magn. Mater. 238 (2002) 129.
[4] H. Figiel, A. Budziak, J. Żukrowski, G. Fisher, M.T. Kelemen, E. Dormann, J. Alloys Compd. 335 (2002) 48.
[5] H. Figiel, A. Budziak, P. Zachariasz, J. Żukrowski, G. Fisher, E. Dormann, J. Alloys Compd. 368 (2004) 260.
[6] H. Figiel, A. Budziak, J. Żukrowski, Solid State Commun. 111 (1999) 519–524.
[7] A. Budziak, P. Zachariasz, L. Kolwicz-Chodak, H. Figiel, A. Pacyna, J. Żukrowski, J. Alloys Compd. 509 (2011) 1347, 1354.
[8] A. Budziak, M. Żurek, J. Żukrowski, M. Balanda, A. Pacyna, M. Czapla, J. Magn. Magn. Mater. (2011), doi:10.1016/j.jmmm.2011.09.007.
[9] A. Somenkov, A.V. Irodova, J. Less-Common Met. 101 (1984) 481.
[10] A. Budziak, H. Figiel, J. Żukrowski, E. Gratz, B. Ouladdiaf, J. Phys. Condens. Matter 13 (2001) L871.
[11] H. Figiel, A. Budziak, J. Żukrowski, G. Wiesinger, B. Ouladdiaf, J. Magn. Magn. Mater. 272–276 (2004) 585–586.
[12] K.P. Yvon, P. Fisher, in: L. Schlapbach (Ed.), Hydrogen in Intermetallic Compounds I, Springer, Berlin, 1988.
[13] H. Figiel, S. Osuchowski, A. Paja, Phys. Status Solidi A 204 (10) (2007) 3286.
[14] H. Wada, H. Nakamura, Y. Yoshimura, M. Shiga, Y. Nakamura, J. Magn. Magn. Mater. 70 (1987) 134.
[15] M.D. Nunez Regueiro, C. Lacroix, J. Magn. Magn. Mater. 140–144 (1995) 1753.
[16] N.H. Kim-Ngan, F.F. Bekker, P.E. Brommer, J.M. Franse, Physica B 160 (1990) 388–392.
[17] B. Ouladdiaf, R. Ballou, J. Deportes, R. Lemaire, F. Sayetat, J. Phys. Condens. Matter 4 (1992) 4675–4686.
[18] Y. Tagawa, J. Sakurai, Y. Komura, H. Wada, M. Shiga, Y. Nakamura, J. Phys. Soc. Jpn. 54 (1985) 591–597.
[19] J. Żukrowski, M. Strecker, G. Wortmann, J. Przewoźnik, K. Krop, J. Alloys Compd. 261 (1997) 47.
[20] J. Rodrigues-Carvajal, FullProf.2k ver. 4.7, ILL., 2011, http://www.ill.eu/sites/fullprof/php/programs.html.
[21] H.M. Rietveld, Acta Crystallogr. 22 (1967) 151;
H.M. Rietveld, J. Appl. Crystallogr. 2 (1969) 65.
[22] C.E. Housecroft, A.G. Sharpe, Inorganic Chemistry, 2nd ed., Prentice Hall, 2004, pp. 536, 649, 743.
[23] I.N. Goncharenko, I. Mirebeau, A.V. Irodowa, E. Suard, Phys. Rev. B 59 (1999) 9324.
[24] M. Latroche, V. Paul-Boncour, A. Percheron-Guégan, F. Bourée-Vigneron, J. Alloys Compd. 274 (1998) 59–64.
[25] A. Budziak, Unpublished data.